Int. J. Heat Mass Transfer. Vol. 14, pp. 1415–1431. Pergamon Press 1971. Printed in Great Britain

THE RAPID GROWTH OF A VAPOUR BUBBLE AT A LIQUID–SOLID INTERFACE

H. J. VAN OUWERKERK†

Koninklijke/Shell-Laboratorium, Amsterdam, The Netherlands

(*Received* 20 *October* 1970 *and in revised form* 14 *December* 1970)

Abstract—The rapid growth of vapour bubbles at a liquid–solid interface, as in boiling liquids, is described by a self-similar solution. A bubble grows as a hemisphere, the square of the radius increasing proportionally with time, while a thin layer of liquid is left on the solid under the bubble. Evaporation from this layer contributes to the growth rate and creates a dry area at its centre. The theory is illustrated with some experimental results. In the Appendix an analysis is presented of the boundary layer on the solid surface outside the bubble. It is shown that separation of this boundary layer does not occur, which explains the presence of the microlayer.

NOMENCLATURE

a, heat diffusivity [m^2s^{-1}];
c, specific heat [$Jkg^{-1}K^{-1}$];
C, dimensionless parameter;
f, modified stream function;
g, acceleration of gravity [ms^{-2}];
h, microlayer thickness [m];
h_0, original microlayer thickness [m];
h^*, boundary-layer thickness [m];
H, a_s/a_l;
j, dimensionless stream function;
J, $c_l(T_1 - T_0)/L$;
k, growth constant [$ms^{-\frac{1}{2}}$];
K, ρ_l/ρ_v;
L, latent heat of evaporation [Jkg^{-1}];
M, λ_s/λ_l;
n, unit normal;
p, pressure in liquid [Nm^{-2}];
$p(\infty)$, ambient pressure [Nm^{-2}];
p_v, pressure in vapour [Nm^{-2}];
P, Prandtl number v_l/a_l;
Q, dimensionless liquid pressure;
Q_v, dimensionless vapour pressure;
r_b, hemispherical bubble radius [m];
r_c, nucleation cavity radius [m];
r_d, dry area radius [m];
R, Reynolds number $k^2/2v_l$;
S, bubble surface [m^2];
t, time [s];
T, temperature [K];
T_0, saturation temperature [K];
T_1, initial temperature [K];
v, liquid velocity [ms^{-1}];
V, bubble volume [m^3];
w, dimensionless liquid velocity;
Z_b, dimensionless constant;
r, spherical coordinate [m];
ϑ, spherical coordinate;
$\tilde{r}$, cylindrical coordinate [m];
$\tilde{z}$, cylindrical coordinate [m];
α, dimensionless spherical coordinate;
$\tilde{\alpha}$, $\tilde{\eta}$, η, ζ, dimensionless cylindrical coordinates;
α_d, dimensionless dry area radius;
β, dimensionless microlayer thickness;
γ, dimensionless microlayer thickness;
λ, heat conductivity [$Wm^{-1}K^{-1}$];
τ, dimensionless time;
τ_d, dimensionless evaporation time of microlayer;

† Present address: Dept. of Physics, Eindhoven University of Technology, The Netherlands.

θ, dimensionless temperature;
ν_l, kinematic viscosity [$m^2 s^{-1}$];
ρ, density [$kg\,m^{-3}$];
ρ'_v, vapour density at T_1 [$kg\,m^{-3}$];
ρ_v, vapour density at T_0 [$kg\,m^{-3}$];
σ, surface tension [Nm^{-1}].

Subscripts

s, solid;
l, liquid;
v, vapour.

1. INTRODUCTION

IN BOILING liquids bubbles grow at the heating surface where they nucleate from pits and scratches, as described by Bankoff [1]. Until recently bubble growth theories were available only for spherical bubbles in an infinite liquid medium, for example those of Forster and Zuber [2], Plesset and Zwick [3], Birkhoff *et al.* [4] and Scriven [5]. For lack of a more appropriate theory, they were used to evaluate experiments on bubble growth at the heating surface, as in the paper by Cole and Shulman [6].

However, the experiments carried out by Moore and Mesler [7] show that under a bubble growing on a solid surface a thin layer of liquid is present. This so-called microlayer, which influences bubble growth was observed directly by Sharp [8], Torikai [9] and in our own experiments. To detect the microlayer we used a transparent heating surface fitted with a glass prism to exploit the effect of total reflection, in combination with high-speed photography. This is similar to that described by Torikai [9]. The role of the microlayer in bubble growth was successfully demonstrated in a paper by Cooper [10] based on a series of experiments, using tiny resistance thermometers on the heating surface, reported by Cooper and Lloyd [11]. The results on microlayer thickness obtained in our work, which was carried out in the same period, agree with the theoretical value which will be derived here and also confirm the results obtained by Cooper and Lloyd [11], although the two experimental techniques are essentially different. This point is of interest because Sharp [8] and more recently also Jawurek [12] who both used optical interference methods, found a thickness which appears to be at least one order of magnitude smaller.

In this analysis of bubble growth at the heating surface we will start from a more general consideration of the problem structure. This will allow us to simplify many aspects of the problem then confronting us, to avoid unnecessary approximations, and to improve on Cooper's [10] not entirely satisfactory treatment of both microlayer formation and evaporation. Taking into account the heat content of the microlayer liquid, which was neglected by Cooper [10], we can show that this source of heat governs bubble growth, although, paradoxically, total microlayer evaporation requires a large amount of heat to be withdrawn from the solid, a conclusion which is also verified experimentally. These findings explain why the thermal properties of the solid hardly influence the bubble growth rate, a result inferred already by Sernas and Hooper [13] on the basis of their experimental results. Owing to neglect of the heat content of the microlayer liquid, Cooper's [10] expressions for the bubble growth rate are incorrect, even in the extreme case analysed in his paper, and are not therefore the upper and lower limits for the growth rate to be expected in intermediate cases.

2. GROWTH HISTORY OF A BUBBLE

During nucleation and initial growth the pressure inside a bubble is practically equal to the saturation pressure at the prevailing superheat. A nucleation radius r_c requires a certain superheat, which is determined by the surface tension excess pressure. Taking terms $(\rho_l - \rho'_v)/\rho_l$ to be equal to 1, we can write

$$p_v - p(\infty) = \frac{\rho'_v L}{T_1}(T_1 - T_0) = \frac{2\sigma}{r_c}. \qquad (1)$$

When for a spherical bubble the radius r_b

exceeds r_c the surface tension pressure decreases and the difference between the excess vapour pressure and the surface tension pressure can drive growth. For such a spherical bubble the initial growth has been described by Plesset and Zwick [3]. We use their arguments here in a slightly modified form. The Rayleigh equation

$$\frac{1}{\rho_l}[p_v - p(\infty)] = \frac{2\sigma}{r_b\rho_l} + \frac{3}{2}\left(\frac{dr_b}{dt}\right)^2 + r_b\frac{d^2r_b}{dt^2} \qquad (2)$$

can be integrated to give

$$\left(\frac{dr_b}{dt}\right)^2 = \frac{2}{3}\frac{p_v - p(\infty)}{\rho_l}\left[1 - \frac{3}{2}\frac{r_c^3}{r_b^3} + \frac{1}{2}\frac{r_c}{r_b}\right]. \qquad (3)$$

A constant growth rate will be approached but cannot be sustained. The heat which should have gone into the bubble therefore as latent heat is proportional to t^3, increasing more rapidly than the volume of liquid $r_b^2(a_l t)^{\frac{1}{2}} \div t^{\frac{5}{2}}$ from which heat could be withdrawn. The temperature and the vapour pressure therefore decrease, and thereby also the growth rate. Ultimately the temperature in the bubble will hardly differ from the saturation temperature T_0, the vapour density then being practically equal to ρ_v, but at least for some time the dynamical excess pressure is nevertheless still large compared with pressure effects of surface tension and gravity. The growth rate asymptotically approaches a value which is governed by heat transport to the bubble during this so-called stage of rapid growth.† For a spherical bubble this form of growth was described by Birkhoff *et al.* [4]. As we will see the Reynolds number R has a constant large value. The successive stages of growth are also discussed in a numerical study by Waldman and Houghton [14].

† The term rapid growth is used because the volumetric growth rate is highest during this growth phase. Note that this is not true for the linear growth rate, which is highest during initial growth.

In the problem of bubble growth at a solid–liquid interface these different stages of growth can also be distinguished. The beginning and end of the stage of rapid growth are determined by the strong inequalities in Table 1. To describe it we can use a number of unrestrictive simplifying assumptions, neglecting vapour viscosity, pressure differences in the bubble and others which are discussed in detail by Plesset and Zwick [3].

Table 1. Conditions for self-similar solution

Original form	Form for growth $r_b = kt^{\frac{1}{2}}$
$\frac{T_v - T_0}{T_1 - T_0} \ll 1$	$\frac{\rho_l k^4}{8\left(\frac{dp}{dT}\right)_{sat}(T_1 - T_0)r_b^2} \ll 1$
$\frac{\rho_v' - \rho_v}{\rho_v} \ll 1$	$\frac{\rho_l k^4}{8p(\infty)r_b^2} \ll 1$
$\frac{\rho_l g r_b}{p_v - p(\infty)} \ll 1$	$\frac{8gr_b^3}{k^4} \ll 1$
$\frac{2\sigma}{r_b[p_v - p(\infty)]} \ll 1$	$\frac{16\sigma r_b}{\rho_l k^4} \ll 1$

For the case of uniform initial superheat it can be shown that the problem of rapid growth is simpler than expected. When we use spherical polar coordinates r, ϑ and φ, of which φ does not occur owing to symmetry, it is found that the number of independent variables is two and not three, as r and t occur in a certain combination,

$$\alpha = r/kt^{\frac{1}{2}} \qquad (4)$$

only. A self-similar solution with independent variables α and ϑ can describe rapid growth. The governing differential equations are the r and ϑ components of the Navier–Stokes equation in the liquid, the heat diffusion equation in the liquid and the solid, supplemented by a number of homogeneous boundary and symmetry conditions. We further have the heat balance which requires that all heat conducted to the bubble surface at temperature T_0 is used for the evaporation of liquid and

therefore controls the rate of vapour generation and thus of bubble growth.

$$\int_S \lambda_l \nabla T_l \cdot \boldsymbol{n}\,\mathrm{d}S = \rho_v L \frac{\mathrm{d}V}{\mathrm{d}t}. \tag{5}$$

To establish that these equations have a self-similar solution the independent and dependent variables shown in Table 2 must be substituted

Table 2. Variables for self-similar solution

Original variable	Self-similar variable
t	—
r	$\alpha = \dfrac{r}{kt^{\frac{1}{2}}}$
ϑ	ϑ
T	$\theta(\alpha, \vartheta) = \dfrac{T - T_0}{T_1 - T_0}$
v_r	$w_r(\alpha, \vartheta) = \dfrac{v_r t^{\frac{1}{2}}}{k}$
v_ϑ	$w_\vartheta(\alpha, \vartheta) = \dfrac{v_\vartheta t^{\frac{1}{2}}}{k}$
$p - p(\infty)$	$Q(\alpha, \vartheta) = \dfrac{\{p - p(\infty)\}t}{\rho_l k^2}$
$p_v - p(\infty)$	$Q_v = \dfrac{\{p_v - p(\infty)\}t}{\rho_l k^2}$

into the equations. At the same time it is assumed that the bubble surface can be described in the α, ϑ system. Doing so, we find that reformulation in terms of α and ϑ and functions of these is possible, as the variable t disappears from all equations and conditions. The equations obtained in this way are still too difficult to solve directly and are therefore not reproduced here. On this basis some conclusions can be drawn.

(1) The bubble has a fixed surface $\alpha = \alpha_b(\vartheta)$ in the α, ϑ system which implies that the bubble will not change its shape during rapid growth.

(2) The surface is given by

$$r = kt^{\frac{1}{2}}\alpha_b(\vartheta) = r_b^*(\vartheta, t) \tag{6}$$

in the r, ϑ, t system of coordinates, the bubble clearly grows proportionally to $t^{\frac{1}{2}}$

(3) Normalizing the shape factor such that

$$\alpha_b(0) = 1 \tag{7}$$

we obtain k as the growth constant in the direction $\vartheta = 0$, which can be used to define the bubble Reynolds number

$$R = \frac{r_b^*(0, t)\,\mathrm{d}/\mathrm{d}t\,\{r_b^*(0, t)\}}{\nu_l} = \frac{k^2}{2\nu_l} \tag{8}$$

which is constant. As a result of the simplifying assumptions the self-similar solution for rapid growth is valid only when a number of conditions are fulfilled. These have been worked out for growth proportional to $t^{\frac{1}{2}}$ in Table 1, where $r_b = r_b^*(0, t)$. See also Fig. 1 which shows the phase of rapid growth for two cases.

In the following we shall analyse the phase of rapid growth under the idealized conditions that solid and liquid are uniformly superheated at equal temperatures and no heat is generated in the solid. In section 6 we shall see how the results of this analysis can be applied to nucleate boiling.

3. FLOW FIELD AND SHAPE OF THE BUBBLE

When the Reynolds number defined in the previous section has a large value, the local volume increase associated with the evaporation of liquid into the bubble will cause liquid flow resembling inviscid flow, except in a thin layer on the solid surface where a viscous boundary layer develops to satisfy the non-slip condition. The inviscid flow in the main region will be uniformly radial, as there is no preferred direction for such flow in this situation, and the bubble will therefore grow in the form of a hemisphere with radius r_b. Under the bubble a thin layer of liquid, the microlayer, remains on

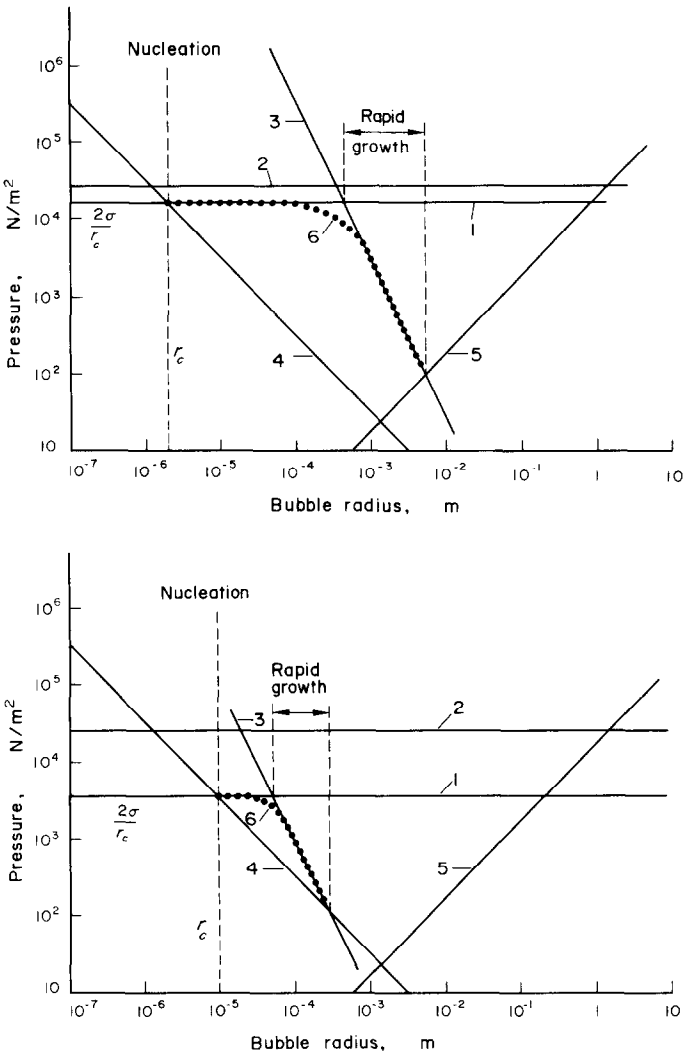

FIG. 1. Pressure effects calculated for bubble growth following $r_b = kt^{\frac{1}{2}}$. Bubble in n-heptane at a uniform superheat of 17·5 K, boiling point 329 K at a pressure of 185 mm Hg = 24·6 kN/m², and a bubble at 4 K superheat.

1. superheat excess pressure $\rho_v L/T_0 (T_1 - T_0)$;
2. ambient pressure $p(\infty)$;
3. dynamical excess pressure $\rho_l k^4/8r_b^2$;
4. surface tension excess pressure $2\sigma/r_b$;
5. pressure difference across bubble due to gravity $\rho_l g r_b$;
6. excess pressure in bubble $p_v - p(\infty)$, qualitatively.

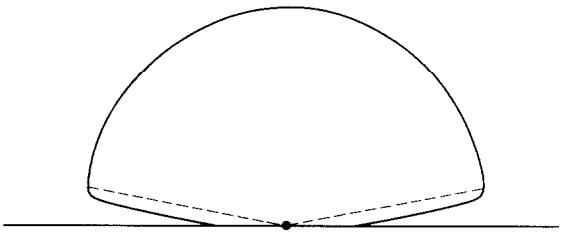

FIG. 2. Shape of the growing bubble.

Broken line indicates thickness of the liquid layer at each point before being decreased by evaporation.

the solid, as shown in Fig. 2. The hemisphere grows as

$$r_b = kt^{\frac{1}{2}}. \tag{9}$$

It can be verified that the liquid outside the bubble will be accelerated everywhere during the initial stage of growth when r_b is proportional to t. During this initial stage flow reversal cannot occur therefore, and a boundary layer type of flow is established. During the stage of rapid growth when the growth rate approaches the value corresponding to $r_b = kt^{\frac{1}{2}}$, the acceleration is negative in a thin shell surrounding the bubble, $1 < (r/r_b) < 2^{\frac{1}{3}}$, as can be seen from the Navier–Stokes equation applied to the main stream region:

$$\frac{\partial v_r}{\partial t} + v_r \frac{\partial v_r}{\partial r} = -\frac{1}{\rho_l}\frac{\partial p}{\partial r} = \frac{k^3}{2r^2 t^{\frac{1}{2}}}\left(\frac{1}{2} - \frac{r_b^3}{r^3}\right). \tag{10}$$

As the flow in the boundary layer, compared with the main flow, is further decelerated by viscous forces, flow reversal at this stage would have to begin by separation of the boundary layer in the region

$$1 < \frac{r^3}{r_b^3} < 2 \quad (1 < \alpha^3 < 2)$$

where the flow must overcome a pressure increase. We will show in the appendix that separation does not occur: Microlayer formation is possible during rapid growth.

The amount of liquid captured under the bubble is determined by the displacement thickness of the boundary layer at $\tilde{r} = r_b$. (In the following cylindrical coordinates $\tilde{r}$, $\tilde{z}$, $\tilde{\varphi}$ will be used in the description of the microlayer.)

As the bubble will not change its shape, the thickness of the microlayer at $\tilde{r} = r_b$ must be proportional to the bubble radius. It must further be proportional to $R^{-\frac{1}{2}}$ because it is derived from a boundary-layer thickness. We have therefore

$$h_0(r_b) = r_b Z_b R^{-\frac{1}{2}}. \tag{11}$$

Although some residual flow is possible where the liquid is captured under the bubble, it will be stopped by viscous forces, and we will assume in the present analysis that the liquid is at rest under the bubble and that the thickness h_0 will change through evaporation of liquid only. The value of Z_b is calculated in the Appendix.

4. EVAPORATION OF THE MICROLAYER, BUBBLE GROWTH RATE

In the calculation of microlayer evaporation a useful simplification is possible. The transient heat flux which occurs when, upon becoming part of the microlayer under the bubble, the liquid is suddenly exposed to evaporation can be shown to be a factor $R^{\frac{1}{2}}$ larger in the $\tilde{z}$ direction than in the $\tilde{r}$-direction. Thus, we assume heat conduction to occur in the $\tilde{z}$ direction only. We must now describe the evaporation of a layer of liquid, at a position $\tilde{r} = \tilde{r}_1$, of thickness h which was initially

$$h = h_0(\tilde{r}_1) \tag{12}$$

at time

$$t_1 = \tilde{r}_1^2 k^{-2} \tag{13}$$

when evaporation begun as a result of a heat flux to the vapour liquid interface where the temperature had suddenly dropped from T_1 to T_0.

In a dimensionless formulation, chosen such that the smallest number of parameters will appear, the problem can be stated as follows.

New variables presented in Table 3 have been

Table 3. Dimensionless variables and parameters for the calculation of microlayer evaporation

Variables	Dimensionless variables
layer thickness h	$\beta = h/h_0$
time $t - t_1$	$\tau = \dfrac{a_l(t - t_1)}{h_0^2}$
position in liquid $\tilde{z}$	$\tilde{\eta} = \dfrac{\tilde{z}}{h_0}$
position in solid $\tilde{z}$	$\tilde{\eta} = \dfrac{\tilde{z}}{h_0} H^{-\frac{1}{2}}$
temperature T	$\theta = \dfrac{T - T_0}{T_1 - T_0}$
Parameters	
$H = \dfrac{a_s}{a} = \dfrac{\lambda_s \rho_l c_l}{\lambda_l \rho_s c_s}$	
$M = \dfrac{\lambda_s}{\lambda_l}$	
$J = \dfrac{c_l(T_1 - T_0)}{L}$	
$P = \dfrac{v_l}{a_l}$	
$K = \dfrac{\rho_l}{\rho_v}$	

defined with the help of the knowledge about the self-similarity of the solution

$$\theta_l = \theta_s = 1 \quad \text{at} \quad \tau = 0 \tag{14}$$

$$\beta = 1 \quad \text{at} \quad \tau = 0 \tag{15}$$

$$\theta_l = 0 \quad \text{at} \quad \tilde{\eta} = \beta \tag{16}$$

$$\theta_s \to 1 \quad \text{when} \quad \tilde{\eta} \to -\infty \tag{17}$$

$$\frac{\partial \theta_l}{\partial \tilde{\eta}} = MH^{-\frac{1}{2}} \frac{\partial \theta_s}{\partial \tilde{\eta}} \quad \text{at} \quad \tilde{\eta} = 0 \tag{18}$$

$$\frac{\partial \theta_l}{\partial \tau} = \frac{\partial^2 \theta_l}{\partial \tilde{\eta}^2} \quad 0 < \tilde{\eta} < \beta \tag{19}$$

$$\frac{\partial \theta_s}{\partial \tau} = \frac{\partial^2 \theta_s}{\partial \tilde{\eta}^2}, \quad \tilde{\eta} < 0 \tag{20}$$

$$\frac{\mathrm{d}\beta}{\mathrm{d}\tau} = J \left(\frac{\partial \theta_l}{\partial \tilde{\eta}} \right)_{\eta = \beta}. \tag{21}$$

These equations can be solved, although in general only numerically, to obtain $\beta = \beta(\tau, J, MH^{-\frac{1}{2}})$, which then yields the value $\tau_d = \tau_d(J, MH^{-\frac{1}{2}})$ for which $\beta = 0$, corresponding to complete evaporation. The vapour production per unit surface area as a function of τ is

$$-\frac{\rho_l}{\rho_v}\frac{\mathrm{d}h}{\mathrm{d}t} = -K\frac{\mathrm{d}\beta}{\mathrm{d}\tau}\frac{a_l}{h_0} = -\frac{a_l}{\tilde{r}_1}\frac{KR^{\frac{1}{2}}}{Z_b}\frac{\mathrm{d}\beta}{\mathrm{d}\tau}. \tag{22}$$

With this function β the situation at the microlayer under the bubble at any given moment can be described. Going from the hemispherical surface towards the bubble centre the evaporation process is further developed, until at a radius $r_d = \alpha_d r_b$ the solid surface is dry. The dimensionless position $\tilde{\alpha}_1 = \tilde{r}_1/r_b$ and τ are related by (9), (11), (12) and the definition of τ in Table 3

$$\tau = \frac{1}{2PZ_b^2}\left(\frac{1}{\tilde{\alpha}_1^2} - 1\right). \tag{23}$$

The total evaporation at the microlayer is then given by

$$-\int_{r_d}^{r_b} \frac{a_l}{\tilde{r}_1}\frac{KR^{\frac{1}{2}}}{Z_b}\frac{\mathrm{d}\beta}{\mathrm{d}\tau} 2\pi\tilde{r}_1 \,\mathrm{d}\tilde{r}_1$$

$$= -2\pi a_l r_b KPZ_b R^{\frac{1}{2}} \int_0^{\tau_d} \frac{\mathrm{d}\beta}{\mathrm{d}\tau}(1 + 2PZ_b^2\tau)^{-\frac{3}{2}}\,\mathrm{d}\tau. \tag{24}$$

Together with the evaporation at the hemispherical surface, which was calculated by Birkhoff *et al.* [4], this must equal the volume increase of the bubble

$$2\pi r_b^2 \frac{\mathrm{d}r_b}{\mathrm{d}t} = -2\pi a_l r_b KPZ_b R^{\frac{1}{2}} \int_0^{\tau_d} \frac{\mathrm{d}\beta}{\mathrm{d}\tau} \times (1 + 2PZ_b^2\tau)^{-\frac{3}{2}}\,\mathrm{d}\tau + 2\pi a_l r_b \pi^{-\frac{1}{2}}(\sqrt{6})\, KP^{\frac{1}{2}}R^{\frac{1}{2}}J. \tag{25}$$

The bubble growth rate is thus

$$R^{\frac{1}{2}} = -KZ_b \int_0^{\tau_d} \frac{d\beta}{d\tau}(1 + 2PZ_b^2\tau)^{-\frac{3}{2}}\,d\tau + \pi^{-\frac{1}{2}}(\sqrt{6})\,KJP^{-\frac{1}{2}}. \quad (26)$$

5. ANALYTICAL SOLUTION FOR A SPECIAL CASE, A USEFUL APPROXIMATION

An interesting aspect is revealed when the identity

$$1 = \int_0^1 \frac{d\beta}{d\tau}\,d\tau + \int_1^{\tau_d} \frac{d\beta}{d\tau}\,d\tau \quad (27)$$

and the integral I in (26)

$$I = \int_0^1 \frac{d\beta}{d\tau}(1 + 2PZ_b^2\tau)^{-\frac{3}{2}}\,d\tau + \int_1^{\tau_d} \frac{d\beta}{d\tau}(1 + 2PZ_b^2\tau)^{-\frac{3}{2}}\,d\tau \quad (28)$$

are compared. $\tau = 1$ corresponds to the time or position at which the penetration distance for heat diffusion is so much less than twice the microlayer thickness that the thermal properties of the solid have not yet had a noticeable influence on microlayer evaporation. At the values of the superheat normally found only a small fraction of the heat needed to evaporate the liquid is supplied by its own heat content, and the second integral in (27) is therefore larger than the first. Nevertheless, in (28), when $PZ_b^2 \gg 1$, the first integral will be the larger one. It can be concluded that although the thermal properties of the solid have an important influence on the total evaporation of the microlayer, and thus on the radius of the dry area under the bubble, which is

$$r_d = \alpha_d r_b = (1 + 2PZ_b^2\tau_d)^{-\frac{1}{2}} r_b, \quad (29)$$

they hardly affect the bubble growth rate because the outer ring of the microlayer, where no heat has yet been withdrawn from the solid, is wide and has moreover a large circumference. This explains an apparent contradiction which emerged from our experiments, as will be discussed in section 6.

An important consequence of these findings is that the analytical solution for

$$MH^{-\frac{1}{2}} = \left(\frac{\lambda_s\rho_s c_s}{\lambda_l\rho_l c_l}\right)^{\frac{1}{2}} = 1$$

provides a good approximation for the bubble growth rate, although it is useless for predicting the dry area radius under the bubble. This analytical solution, also a self-similar one, was obtained by Knuth [15]. In terms of the independent variable ζ,

$$\zeta = \frac{1 - \tilde{\eta}}{2\tau^{\frac{1}{2}}} \quad (30)$$

and one parameter C

$$C = \frac{1 - \beta}{2\tau^{\frac{1}{2}}} \quad (31)$$

given by

$$J\pi^{\frac{1}{2}} = C\,e^{C^2}\,\mathrm{erfc}\,C \quad (32)$$

the solution is

$$\theta = \frac{\mathrm{erfc}\,C - \mathrm{erfc}\,\zeta}{\mathrm{erfc}\,C}. \quad (33)$$

We thus have

$$\beta = 1 - 2C\tau^{\frac{1}{2}} \quad (34)$$

$$\frac{d\beta}{d\tau} = -\frac{C}{\tau^{\frac{1}{2}}} \quad (35)$$

$$\tau_d = (4C^2)^{-1} \quad (36)$$

and the expression (26) now becomes

$$R^{\frac{1}{2}} = KZ_b\left(1 + \frac{2PZ_b^2}{4C^2}\right)^{-\frac{1}{2}} + \pi^{-\frac{1}{2}}(\sqrt{6})\,KJP^{-\frac{1}{2}}. \quad (37)$$

This solution is compared with the results of a numerical calculation in Fig. 3. Equations (14)–(21) were solved numerically to obtain the

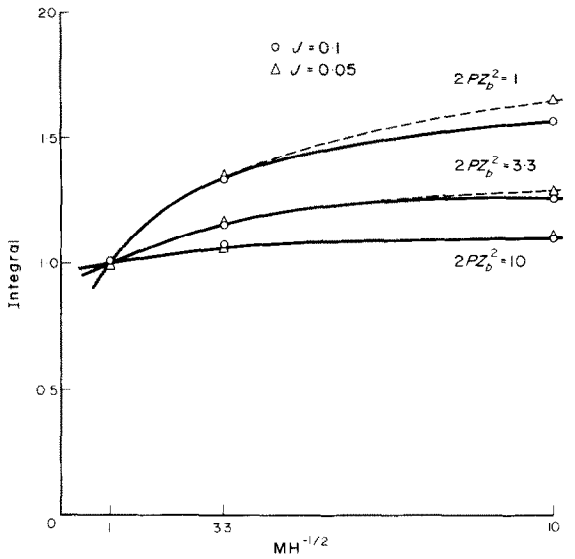

FIG. 3. Numerically calculated values of the integral

$$-\left(1+\frac{PZ_b^2}{2C^2}\right)^{\frac{1}{2}}\int_0^{\tau_d}\frac{d\beta}{d\tau}(1+2PZ_b^2)^{-\frac{1}{2}}\,d\tau.$$

The ratio of the first terms in (26) and (37) to compare numerical and analytical solutions.

integral in (26) and the value of τ_d for various values of the parameters $2PZ_b^2$ and $MH^{-\frac{1}{2}}$. The values for τ_d are shown in Fig. 4. These numerical results will be used to evaluate the observed values of growth rate and dry area radius.

When J is small we have approximately

$$C = J\pi^{-\frac{1}{2}} \tag{38}$$

and when also PZ_b^2 is not too small (37) reduces to

$$R^{\frac{1}{2}} = \pi^{-\frac{1}{2}}(\sqrt{2})\,KJP^{-\frac{1}{2}}(1+\sqrt{3}). \tag{39}$$

It is interesting to note that in the approximation for microlayer evaporation corresponding to equations (14)–(21) the hemispherical and microlayer surfaces are joined smoothly. At the outer ring of the microlayer the evaporation is described in this approximation by (31), from which the shape of the microlayer surface can be calculated. The thickness is

$$\gamma = \frac{h}{r_b} = Z_b R^{-\frac{1}{2}}\tilde{\alpha}(1-2C\tau^{\frac{1}{2}}) \tag{40}$$

or

$$\gamma = Z_b R^{-\frac{1}{2}}\tilde{\alpha} - C(\sqrt{2P})^{-\frac{1}{2}}R^{-\frac{1}{2}}(1-\tilde{\alpha}^2)^{\frac{1}{2}}. \tag{41}$$

When $\tilde{\alpha}$ approaches 1 from below the derivative $d\gamma/d\tilde{\alpha}$ becomes infinite; thus the tangents to the hemispherical and microlayer surfaces have the same direction where these surfaces meet.

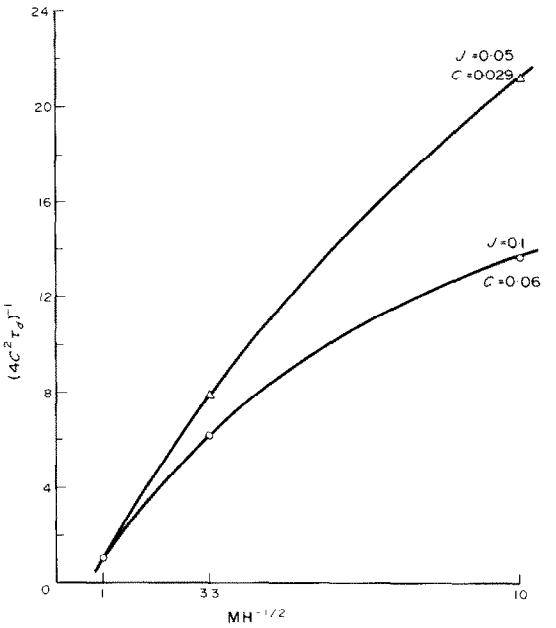

FIG. 4. Dimensionless time interval τ_d necessary for complete evaporation of the thin liquid layer, calculated numerically.

6. APPLICATION TO NUCLEATE BOILING

In nucleate pool boiling at low pressures with a small constant external heat input there is a large time interval between the nucleation of subsequent bubbles. During this interval the heat from the external source is partly accumulated in the solid, replacing the heat lost to the preceding bubble, while a relatively small amount of heat is conducted into the liquid. The bulk of the liquid is at the saturation temperature and the liquid near the solid will be super-

heated. When the replacement of the lost heat has been completed the heat conduction becomes almost stationary, so the solid will have a practically uniform temperature. Obviously, the liquid in direct contact with it has the same temperature and a temperature gradient is found in the liquid. The temperature field will be indicated by $T_l(\tilde{z})$, with $T_l(0) = T_1$.

At that moment the next bubble emerges from its nucleation cavity. After the initial phase of growth when the dynamical excess pressure inside is at its maximum corresponding to the liquid superheat it enters the period of rapid growth. If it is assumed that the bubble grows according to expression (9), the theory developed in the foregoing describes the heat conduction and the evaporation at the liquid layer under the bubble. The initial conditions near the solid–liquid interface are the same as those in section 4. The temperature drop across a distance of the order of the extremely small microlayer thickness, which is a result of the thermal gradient in the liquid, can be neglected, while it can be shown that the small external heat input is negligible in comparison with the transient heat flux given by (21) and (35) until the bubble has grown to very large dimensions. The contribution to growth of the evaporation at the hemispherical surface is different, however, from the contribution found in the case of uniformly superheated liquid.

The temperature field in the liquid affects this contribution in two different ways. In terms of spherical polar coordinates the variation of temperature with radial position will have an influence which is negligible at first, but the cause of a deviation from equation (9) later. Before this deviation occurs the variation of temperature with ϑ will not change with time and influence relation (9) through the value of k only.

We will first discuss the consequences of a radial variation of temperature. At the hemispherical surface of a bubble growing rapidly at a liquid–solid interface under conditions of uniform initial superheat a radial temperature gradient extends in the liquid to

$$r = r_b + \Delta r_b \tag{42}$$

where Δr_b is given by

$$\Delta r_b = a_l^{\frac{1}{2}} k^{-1} r_b = r_b \frac{1}{\sqrt{2}} R^{-\frac{1}{2}} P^{-\frac{1}{2}}. \tag{43}$$

When there is an initial radial temperature gradient in the liquid, this will affect the growth relation (9) only when this gradient, which is enhanced in the radial direction by the flow field, becomes comparable in magnitude with the temperature gradient associated with the self-similar solution, which itself decreases proportionally to $t^{-\frac{1}{2}}$ in view of (43). Therefore during a short time interval growth will occur according to (9), after which a deviation from this relation will be observed. (For a spherical bubble this has been shown quantitatively by Skinner and Bankoff [16].)

We now restrict our attention to the time interval during which (9) holds, having to account for the influence of the variation of initial temperature with ϑ in this interval. A bubble emerging from a nucleation cavity has a finite radius before rapid growth starts. At the beginning of growth the liquid at a short distance outside the bubble has a temperature distribution ranging with varying ϑ from the temperature of the solid at the base of the bubble to a lower temperature at the top of the bubble. This temperature distribution remains unchanged in the uniformly radial flow field, as the distance between neighbouring liquid volumes at equal distances from the hemispherical bubble boundary increases proportionally to $kt^{\frac{1}{2}}$, while the penetration distance for heat diffusion is proportional to $(a_l t)^{\frac{1}{2}}$. The ratio of these quantities, which is $(2PR)^{\frac{1}{2}}$, is large. The liquid superheat which governs the local rate of evaporation is thus constant for given ϑ. As a consequence the rate of vapour generation from the entire hemispherical surface could be calculated by using an average value of J, which is constant with time, in the last term of equation (26). The relation (9) is in-

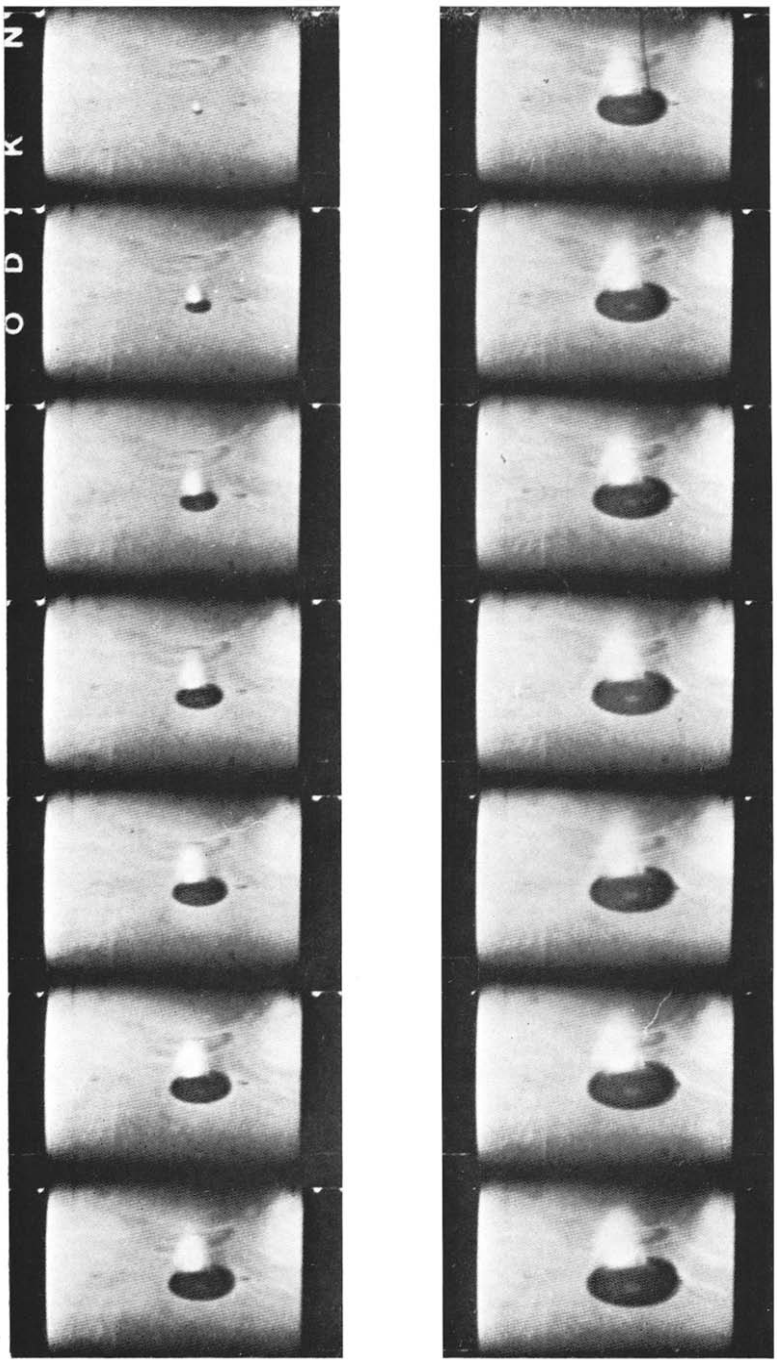

FIG. 5. Growth of a bubble on the Pyrex glass plate. Series of frames of film made with a high-speed camera. The liquid layer and the dry area under the bubble are visible as explained in the text.

fluenced therefore through the value of the constant k only until the radial temperature causes a deviation. A consequence of the geometry of the sphere is that the average replacing J can be expressed as

$$J' = \frac{c_l}{L}\frac{1}{r_{b,0}}\int_0^{r_{b,0}} [T_l(\tilde{z}) - T_0]\,\mathrm{d}\tilde{z} \qquad (44)$$

where $r_{b,0}$ is the radius of the bubble at the beginning of rapid growth. Note that the temperature distribution over ϑ can in principle be measured when the bubble has grown to a much larger size than that which it has at the beginning of rapid growth.

As we have shown that growth according to (9) can be observed in nucleate boiling, we will discuss here some experimental results as an illustration of the theory developed in the foregoing.

Growth rates of a large number of bubbles growing on a transparent heating surface were determined with a high-speed film camera. The heating surface was a Pyrex-glass or a Perspex plate of 20 mm thickness heated electrically by an electroconductive gold layer of 10 nm on the side in contact with the liquid. As liquids we used n-heptane, benzene and carbon tetrachloride at reduced pressures. To enable observation of the liquid layer under the bubble and the dry area at its centre we used ground surfaces and a glass prism: see Figs. 5 and 6.

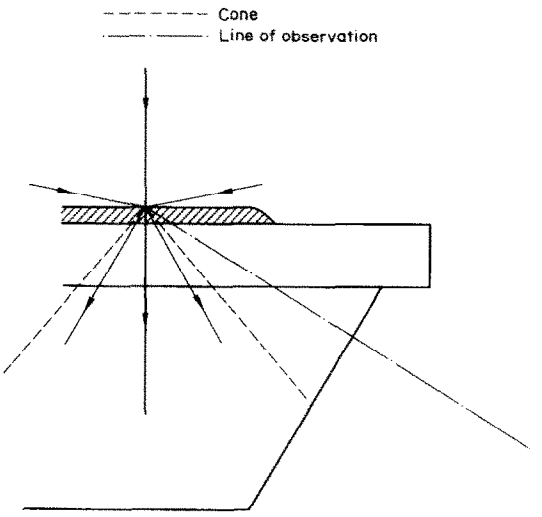

FIG. 6. Reversed effect of total reflection to detect presence of microlayer.

Table 4. Growth rates of vapor bubbles

Liquid	n-Heptane	n-Heptane	n-Heptane	n-Heptane	Benzene	Carbon tetrachloride
Heating surface	Pyrex	Pyrex	Pyrex	Perspex	Pyrex	Pyrex
Pressure (kN/m²)	16·6	16·6	24·6	24·6	30	23·3
(mm Hg)	125	125	185	185	228	175
Boiling point (K)	318	318	329	329	319	308
Superheat (K)	18	19	18	16	26	27
J	0·105	0·11	0·107	0·095	0·108	0·07
$MH^{-\frac{1}{2}}$	3·3	1·3	3·3	1·3	3·2	4·2
K	1080	1080	755	755	966	1900
P	4·0	4·0	3·8	3·8	4·4	5·5
$R^{\ddagger}_{\text{anal}}$ $J' = 0$	45	47	33	29	40	45
$J' = \frac{1}{3}J$	71	74	52	46	63	71
$R^{\ddagger}_{\text{num}}$ $J' = 0$ $Z_b = 0{\cdot}6$	55	51	41	32	48	52
$J' = \frac{1}{3}J$ $Z_b = 0{\cdot}6$	81	78	60	49	71	78
R_{observed} average	82	67	62	52	73	55
Individual values of $R^{\ddagger}$	78–73–73–75–115–100	60–53–72–61	43–94–59	51–53–37	70–76	55
	85–92–50–70–92–78	62–84–75	61–51	46–70–55		

Plots of the squared bubble radius r_b^2 vs. time yielded straight lines over the interval 1 mm $< r_b <$ 2 mm for all bubbles, while for many bubbles the straight lines extended beyond this range. The slope of these lines yields the growth constant. Table 4 presents the values found and compares them with the results of the approximate analytical calculation, equation (37). The results of the numerical solution, obtained from Fig. 3 with $Z_b = 0{\cdot}6$, have also been included. $Z_b = 0{\cdot}6$ is in the middle of the range of values obtained from theory and experiment. The value of J', defined in (44), is clearly different for each individual bubble. Putting $J' = \frac{1}{3}J$, we obtain reasonable agreement between the calculated growth rate and the average of a number of values obtained experimentally.

It proved difficult to determine the value of the dimensionless constant Z_b from the ratio of bubble radius and dry area radius with (29). Measurement from the films of the dry area radius is useful only in the range 1 mm $< r_d <$ 2 mm where the bubble boundary has passed at the velocity corresponding to $r_b = kt^{\frac{1}{2}}$. In this range effects of surface roughness and constant electrical heat input do not play any role. Many bubbles, especially on Perspex, leave the heating surface before the dry area has grown to this size. Straight-line plots of r_d^2 vs. t were obtained, by drawing a line matching the plotted data as closely as possible. See the plots of Fig. 7 for the bubble in Fig. 5. Its slope, divided by the slope of r_b^2 vs. t yields α_d^2. The values obtained for Z_b, between 0·3 and 0·8, are presented in Table 5. Their order of magnitude agrees with the value 0·9 predicted in the appendix. From more direct measurements by Cooper and Lloyd [11] values between 0·4 and 0·7 can be calculated. Although the spread in the experimental values is too large to reach a final conclusion, it appears that the experimental values are lower than the theoretical one. This can be understood when it is considered that the experimental values of Z_b are all calculated on the assumption that the original thickness of

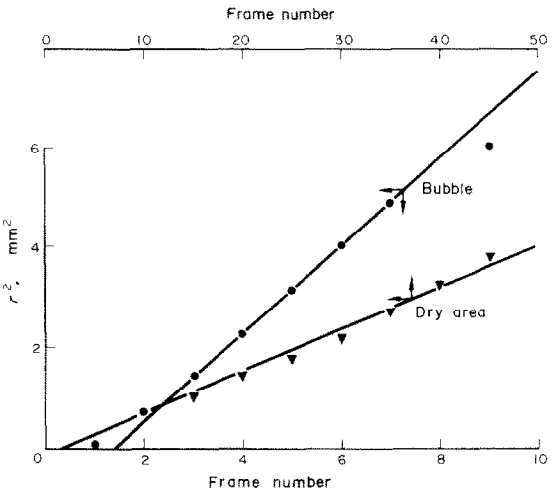

FIG. 7. Bubble radius and dry area radius as a function of time. Bubble of Fig. 5. Time between frames 288 μs.

the microlayer is equal to the total amount of liquid evaporated. Formally the amount carried away by the residual flow should be added to this.

Note that Table 4 shows the bubble growth rate to be hardly dependent on the value of the parameter

$$MH^{-\frac{1}{2}} = \left(\frac{\lambda_s \rho_s c_s}{\lambda_l \rho_l c_l}\right)^{\frac{1}{2}},$$

whereas the value of a_d^{-2} in Table 5 is much larger on Perspex than on Pyrex. This indicates that the thermal properties of the solid have a small influence on the bubble growth rate but affect dry area radius considerably, which confirms the arguments at the beginning of section 5.

7. CONCLUDING REMARKS

The end of the phase of rapid growth remains an interesting subject for further study. At the latest the end will come when one of the last two conditions in Table 1 is no longer satisfied. An earlier end is also possible. When growth slows down, at the moment when the influence of the radial component of a temperature

Table 5. Experimental values of Z_b

Liquid	n-Heptane	n-Heptane	Benzene	Carbon tetrachloride
Heating surface	Pyrex	Perspex	Pyrex	Pyrex
Pressure (kN/m^2)	24·6	16·6	30·0	23·3
(mm Hg)	185	125	228	175
Boiling point (K)	329	318	319	308
Superheat (K)	18	19	26	27
J	0·107	0·11	0·108	0·07
$MH^{-\frac{1}{2}}$	3·3	1·3	3·2	4·2
K	755	1080	966	1900
P	3·8	4·0	4·4	5·5
$R^{\frac{1}{2}}_{num}$ with $J' = \frac{1}{3}J$	60	78	71	78
$R^{\frac{1}{2}}_{observed}$	60	71	76 70	55
$\alpha_{d,\,observed}$	10·5	~160	19 18·2	31
τ_d from Fig. 4	11	~33	10	17
Z_b from α_d	0·34	~0·78	0·45 0·44	0·39
Z_b theor.	~0·9	~0·9	~0·9	~0·9

gradient initially present in the liquid becomes noticeable, separation of the boundary layer could occur. The decrease in dynamical pressure resulting from the reduction in growth rate will further increase the relative importance of surface tension and gravity. According to all these mechanisms the bubble will lose contact with the solid surface, the main heat source for growth. Following the reduction in growth rate growth will thus stop almost entirely.

When effects of surface tension are important the self-similar solution is not applicable. As the observed growth is adequately described by the self-similar solution, surface tension cannot play an important role in it. This contrasts with a suggestion by Cooper and Lloyd [11] that surface tension influences the flow near the junction of the hemispherical and microlayer surfaces.

It should be noted that the same treatment as given above will also apply to bubble growth at the heating surface in a binary mixture if the surface tension gradient, resulting from the concentration gradient along the microlayer, does not induce strong flow in it. The equations for this problem can easily be derived with the help of Scriven's paper [5].

ACKNOWLEDGEMENTS

Helpful suggestions by Professor G. K. Batchelor, University of Cambridge, and valuable comments on the manuscript by Professor D. A. de Vries and Dr. S. J. D. van Stralen of the Eindhoven University of Technology are gratefully acknowledged. I wish to thank Dr. H. L. Beckers of this laboratory for the stimulating discussions in the course of this work.

REFERENCES

1. S. G. Bankoff, The prediction of surface temperatures at incipient boiling, *Chem. Engng Prog. Symp. Ser.* **29**, 87 (1959).
2. H. K. Forster and N. Zuber, Growth of a vapour bubble in a superheated liquid, *J. Appl. Phys.* **25**, 474 (1954).
3. M. S. Plesset and S. A. Zwick, The growth of vapour bubbles in superheated liquids, *J. Appl. Phys.* **25**, 493 (1954).
4. G. Birkhoff, R. S. Margulies and W. A. Horning, Spherical bubble growth, *Physics Fluids* **1**, 201 (1958).
5. L. E. Scriven, On the dynamics of phase growth, *Chem. Engng Sci.* **10**, 1 (1959).
6. R. Cole and H. L. Shulman, Bubble growth rates at high Jakob numbers, *Int. J. Heat Mass Transfer* **9**, 1377 (1966).
7. F. D. Moore and R. B. Mesler, The measurement of rapid surface temperature fluctuations during nucleate boiling of water, *A.I.Ch.E. Jl* **7**, 620 (1961).
8. R. R. Sharp, The nature of liquid film evaporation during nucleate boiling, NASA TN D-1997 (1964).
9. K. I. Torikai, Heat transfer in contact area of a boiling bubble on a heating surface, *Bull. JSME* **10**, 338 (1967).

10. M. G. COOPER, The microlayer and bubble growth in nucleate pool boiling, *Int. J. Heat Mass Transfer* **12**, 915 (1969).
11. M. G. COOPER and A. J. P. LLOYD. The microlayer in nucleate pool boiling, *Int. J. Heat Mass Transfer* **12**, 895 (1969).
12. H. H. JAWUREK, Simultaneous determination of microlayer geometry and bubble growth in nucleate boiling, *Int. J. Heat Mass Transfer* **12**, 843 (1969).
13. V. SERNAS and F. C. HOOPER, The initial vapour bubble growth on a heated wall during nucleate boiling, *Int. J. Heat Mass Transfer* **12**, 1627 (1969).
14. L. A. WALDMAN and G. HOUGHTON, Spherical phase growth in superheated liquids, *Chem. Engng Sci.* **20**, (1965).
15. E. L. KNUTH, Non-stationary phase changes involving a condensed phase and a saturation vapour, *Physics Fluids* **2**, 84 (1959).
16. L. A. SKINNER and S. G. BANKOFF, Dynamics of vapour bubbles in spherically symmetric temperature fields of general variation, *Physics Fluids* **7**, 1 (1964).
17. R. R. OLANDER and R. G. WATTS, An analytical expression of microlayer thickness in nucleate boiling, *J. Heat Transfer* **91C**, 178 (1969).

APPENDIX

In this appendix the flow field around the bubble is studied more closely, the aim being to calculate the constant Z_b and to establish that separation of the boundary layer will not occur outside the bubble.

We use cylindrical polar coordinates $\tilde{r}$ and $\tilde{z}$, the positive $\tilde{z}$-axis extending into the liquid perpendicular to the solid surface. The components of the liquid velocity are $\tilde{v}_r$ and $\tilde{v}_z$. The continuity equation

$$\frac{\partial \tilde{v}_r}{\partial \tilde{r}} + \frac{\tilde{v}_r}{\tilde{r}} + \frac{\partial \tilde{v}_z}{\partial \tilde{z}} = 0, \tag{A.1}$$

is identically satisfied when a stream function φ_b is introduced such that

$$\tilde{v}_r = \frac{1}{\tilde{r}} \frac{\partial \varphi_b}{\partial \tilde{z}}, \tag{A.2}$$

and

$$\tilde{v}_z = -\frac{1}{\tilde{r}} \frac{\partial \varphi_b}{\partial r}. \tag{A.3}$$

For large values of R the boundary layer is confined to a narrow region near the solid where

$$\frac{\tilde{z}}{\tilde{r}} = 0(R^{-\frac{1}{4}}). \tag{A.4}$$

Order of magnitude considerations show that the pressure distribution in the boundary layer is that of the main stream region given by (10), r being replaced by $\tilde{r}$ in view of (A.4). The radial component of the Navier–Stokes equations then takes the form

$$\frac{1}{\tilde{r}} \frac{\partial^2 \varphi_b}{\partial \tilde{z} \partial t} - \frac{1}{\tilde{r}^3} \left(\frac{\partial \varphi_b}{\partial \tilde{z}} \right)^2 + \frac{1}{\tilde{r}^2} \frac{\partial \varphi_b}{\partial z} \frac{\partial^2 \varphi_b}{\partial \tilde{z} \partial \tilde{r}} - \frac{1}{\tilde{r}^2} \frac{\partial \varphi_b}{\mathrm{d}\tilde{r}} \frac{\partial^2 \varphi_b}{\mathrm{d}\tilde{z}^2}$$
$$= \frac{k^3}{2\tilde{r}^2 t^{\frac{1}{2}}} \left(\frac{1}{2} - \frac{k^3 t^{\frac{1}{2}}}{\tilde{r}^3} \right) + \nu_l \left[\frac{\partial^2}{\partial \tilde{r}^2} \left(\frac{1}{\tilde{r}} \frac{\partial \varphi_b}{\partial \tilde{z}} \right) \right.$$
$$\left. + \frac{1}{\tilde{r}} \frac{\partial^3 \varphi_b}{\partial \tilde{z}^3} + \frac{1}{\tilde{r}} \frac{\partial}{\mathrm{d}\tilde{r}} \left(\frac{1}{\tilde{r}} \frac{\partial \varphi_b}{\partial \tilde{z}} \right) - \frac{1}{\tilde{r}^3} \frac{\partial \varphi_b}{\partial \tilde{z}} \right]. \tag{A.5}$$

The relative order of magnitude of the terms, after the brackets have been removed, is 1, 1, 1; 1, 1, 1, R^{-1}, 1, R^{-1}, R^{-1}. The small terms will be neglected.

The boundary conditions are

$$\left. \begin{aligned} \tilde{v}_r &= 0 \\ \tilde{v}_z &= 0 \end{aligned} \right\} \quad \text{at} \quad \tilde{z} = 0, \tag{A.6}$$

and

$$\tilde{v}_r \to v_{r,m} = \frac{k^3 t^{\frac{1}{2}}}{2\tilde{r}^2} \text{ at the top of the boundary layer} \tag{A.7}$$

where the velocity approaches that of the main stream.

Using the self-similarity of the solution we introduce new independent variables

$$\tilde{\alpha} = \frac{\tilde{r}}{kt^{\frac{1}{4}}}, \tag{A.8}$$

$$\eta = \frac{\tilde{z}}{kt^{\frac{1}{4}}} (\tfrac{1}{2}R)^{\frac{1}{4}} = \frac{\tilde{z}}{(4\nu_l t)^{\frac{1}{4}}}, \tag{A.9}$$

and a new dependent variable $j(\tilde{\alpha}, \eta)$ such that

$$\varphi_b = \frac{k^3 t^{\frac{1}{2}}}{2\tilde{\alpha}} (\tfrac{1}{2}R)^{-\frac{1}{4}} j(\tilde{\alpha}, \eta). \tag{A.10}$$

The boundary conditions (A.6) and (A.7) are satisfied when

$$\left. \begin{aligned} j &= 0 \\ \frac{\partial j}{\partial \eta} &= 0 \end{aligned} \right\} \quad \text{at} \quad \eta = 0, \tag{A.11}$$

and

$$\frac{\partial j}{\partial \eta} \to 1 \quad \text{when} \quad \eta \to \infty. \tag{A.12}$$

Equation (A.5) becomes

$$\frac{\partial^2 j}{\partial \eta^3} + 2\tilde{\alpha} \frac{\partial^2 j}{\partial \tilde{\alpha} \partial \eta} + 2\eta \frac{\partial^2 j}{\partial \eta^2} - 2 \frac{\partial j}{\partial \eta} + 2 + \frac{1}{\tilde{\alpha}^3} \left[4 \left(\frac{\partial j}{\partial \eta} \right)^2 \right.$$
$$\left. - 4 - 2\tilde{\alpha} \frac{\partial j}{\partial \eta} \frac{\partial^2 j}{\partial \eta \partial \tilde{\alpha}} + 2\tilde{\alpha} \frac{\partial j}{\partial \tilde{\alpha}} \frac{\partial^2 j}{\partial \eta^2} - 2j \frac{\partial^2 j}{\partial \eta^2} \right] = 0. \tag{A.13}$$

Its form suggests a procedure of successive approximations for large $\tilde{\alpha}^3$. Putting

$$j = \int_0^\eta f_0(\xi)\, \mathrm{d}\xi + \frac{1}{\tilde{\alpha}^3} \int_0^\eta f_1(\xi)\, \mathrm{d}\xi + \ldots, \tag{A.14}$$

the first of the conditions (A.11) is satisfied and (A.13) becomes

$$\frac{d^2f_0}{d\eta^2} + 2\eta\frac{df_0}{d\eta} - 2f_0 + 2 + \frac{1}{\tilde{\alpha}^3}\left[\frac{d^2f_1}{d\eta^2} + 2\eta\frac{df_1}{d\eta} - 8f_1 + 4f_0^2 - 4 - 2\frac{df_0}{d\eta}\int_0^\eta f_0(\xi)\,d\xi\right] + \frac{1}{\tilde{\alpha}^6}[\ldots] + \ldots = 0, \tag{A.15}$$

with the conditions

$$f_0 = 0, \quad f_1 = 0, \quad \ldots \quad \text{at} \quad \eta = 0, \tag{A.16}$$

$$f_0 = 1, \quad f_1 = 0, \quad \ldots \quad \text{at} \quad \eta = \infty. \tag{A.17}$$

Owing to the last condition the solution will satisfy (A.12) for all values of $\tilde{\alpha}$. The zero order solution is

$$f_0 = 1 - \pi^{\frac{1}{2}}\, i\,\mathrm{erfc}\,\eta \tag{A.18}$$

where $i\,\mathrm{erfc}\,\eta$ denotes the first integral of the complementary error function of η. The homogeneous part of the first-order equations has the solutions $i^4\,\mathrm{erfc}\,\eta$ and $i^4\,\mathrm{erfc}\,(-\eta)$, these being fourth integrals of the complementary error function. The solution of the complete equation can be obtained with the method of variation of the constants. Putting

$$f_1 = A(\eta)i^4\,\mathrm{erfc}\,\eta + B(\eta)i^4\,\mathrm{erfc}\,(-\eta) \tag{A.19}$$

we have the conditions

$$\frac{dA}{d\eta}i^4\,\mathrm{erfc}\,\eta + \frac{dB}{d\eta}i^4\,\mathrm{erfc}\,(-\eta) = 0 \tag{A.20}$$

$$-\frac{dA}{d\eta}i^3\,\mathrm{erfc}\,\eta + \frac{dB}{d\eta}i^3\,\mathrm{erfc}\,(-\eta) = 4 - 4f_0^2 + 2\frac{df_0}{d\eta}\int_0^\eta f_0(\xi)\,d\xi \tag{A.21}$$

which determine $dA/d\eta$ and $dB/d\eta$. With two constants, determined by the boundary conditions, $A(\eta)$ and $B(\eta)$ can then be found. To find the thickness of the boundary layer and to determine whether separation will occur in the region $\tilde{\alpha} > 1$, it is not necessary to obtain the solution completely.

Separation of the boundary layer is characterized by the reversal of the direction of flow at the solid surface. Thus the point of separation is determined by the condition

$$\left(\frac{\partial \tilde{v}_r}{\partial \tilde{z}}\right)_{\tilde{z}=0} = 0,$$

which is equivalent to

$$\frac{df_0}{d\eta} + \frac{1}{\tilde{\alpha}^3}\frac{df_1}{d\eta} = 0 \quad \text{at} \quad \eta = 0, \tag{A.22}$$

when terms containing higher powers of α^{-3} are neglected. Consider the solution (A.19) of the first-order equation. As

$$i^4\,\mathrm{erfc}\,(-\eta) \to \infty \quad \text{for} \quad \eta \to \infty,$$

we have

$$B(\infty) = 0$$

in view of (A.17). But then

$$B(\eta) = -\int_\eta^\infty \frac{dB}{d\eta}\,d\eta, \tag{A.23}$$

and as

$$A(0) = -B(0), \tag{A.24}$$

in view of condition (A.16), we have

$$A(0) = \int_0^\infty \frac{dB}{d\eta}\,d\eta. \tag{A.25}$$

From the conditions (A.20) and (A.21) we have

$$\frac{dB}{d\eta} = 4\frac{\{1 - (1 - \pi^{\frac{1}{2}}i\,\mathrm{erfc}\,\eta)^2 + \frac{1}{2}\pi^{\frac{1}{2}}\,\mathrm{erfc}\,\eta\,(\eta + \pi^{\frac{1}{2}}i^2\,\mathrm{erfc}\,\eta - \frac{1}{4}\pi^{\frac{1}{2}})\}i^4\,\mathrm{erfc}\,\eta}{i^4\,\mathrm{erfc}\,(-\eta)i^3\,\mathrm{erfc}\,\eta + i^3\,\mathrm{erfc}\,(-\eta)i^4\,\mathrm{erfc}\,\eta}. \tag{A.26}$$

Repeated partial integrations, combined with the use of recurrence relations and differentiation formulas for the integrals of the complementary error function, then yield with (A.25)

$$A(0) = \frac{248}{15} - \frac{27\pi}{8}. \tag{A.27}$$

With (A.24) and (A.20) we have from (A.19)

$$\left(\frac{df_1}{d\eta}\right)_{\eta=0} = -2A(0)i^3\,\mathrm{erfc}\,(0) = -\frac{A(0)}{3\pi^{\frac{1}{2}}}. \tag{A.28}$$

The condition for separation (A.22) is then

$$\pi^{\frac{1}{2}} - \frac{1}{3\pi^{\frac{1}{2}}\tilde{\alpha}^3}\left(\frac{248}{15} - \frac{27\pi}{8}\right) = 0. \tag{A.29}$$

A point of separation is therefore not found in the region $\tilde{\alpha} > 1$ outside the bubble. The result $\tilde{\alpha}^3 \simeq 0{\cdot}63$ from (A.29) is itself meaningless because the analysis is valid outside the bubble only.

The displacement thickness h^* of the boundary layer is defined by the expression

$$h^* = (4\nu_l t)^{\frac{1}{2}}\int_0^\infty \frac{\tilde{v}_{r,m} - \tilde{v}_r}{v_{r,m}}\,d\eta, \tag{A.30}$$

which can be rewritten, if only zero and first-order terms in $\tilde{\alpha}^{-3}$ are retained, as

$$h^* = (4\nu_l t)^{\frac{1}{2}} \int_0^\infty \left(1 - f_0 - \frac{1}{\tilde{\alpha}^3} f_1\right) d\eta$$

$$= (4\nu_l t)^{\frac{1}{2}} \left[\pi^{\frac{1}{2}} \int_0^\infty i\,\mathrm{erfc}\,\eta\, d\eta - \frac{1}{\tilde{\alpha}^3} \times \int_0^\infty \{Ai^4\,\mathrm{erfc}\,\eta + Bi^4\,\mathrm{erfc}\,(-\eta)\}\, d\eta\right]. \quad (A.31)$$

A partial integration of the second integral I_2 yields

$$I_2 = \int_0^\infty \{Ai^4\,\mathrm{erfc}\,\eta + Bi^4\,\mathrm{erfc}\,(-\eta)\, d\eta$$

$$= -\,[Ai^5\,\mathrm{erfc}\,\eta - Bi^5\,\mathrm{erfc}\,(-\eta)]_0^\infty + \frac{1}{10}\int_0^\infty \left\{\frac{dA}{d\eta} i^3\,\mathrm{erfc}\,\eta - \frac{dB}{d\eta} i^3\,\mathrm{erfc}\,(-\eta)\right\} d\eta, \quad (A.32)$$

with the use of the recurrence relations and (A.20). As $B(\infty) = 0$ and $i^5\,\mathrm{erfc}\,(\infty) = 0$, using also (A.24) and (A.21), we obtain

$$I_2 = 2A(0)\, i^5\,\mathrm{erfc}\,(0) - \frac{4}{10}\int_0^\infty \{1 - (1 - \pi^{\frac{1}{2}} i\,\mathrm{erfc}\,\eta)^2 + \tfrac{1}{2}\pi^{\frac{1}{2}}\,\mathrm{erfc}\,\eta\,(\eta + \pi^{\frac{1}{2}} i^2\,\mathrm{erfc}\,\eta - \tfrac{1}{4}\pi^{\frac{1}{2}})\}\, d\eta$$

$$= -\tfrac{1}{4}\pi^{\frac{1}{2}}\left(\frac{9}{4} - \frac{4\sqrt{2}}{5} - \frac{496}{225\pi}\right) \quad (A.33)$$

The final result is

$$\frac{h^*}{(4\nu_l t)^{\frac{1}{2}}} \simeq \tfrac{1}{4}\pi^{\frac{1}{2}}\left(1 + \frac{1}{\tilde{\alpha}^3}.0{\cdot}042\right) \quad (A.34)$$

to the first order in $1/\tilde{\alpha}^3$.

The zero-order term for the thickness of the boundary layer can also be obtained from a very simple calculation. The component of the Navier–Stokes equation along the solid surface can be simplified to a diffusion equation for the difference between actual and main stream velocity, as was done by Olander and Watts (16). But such an approximation, which as they assume is valid for small values of time, is valid only far away from the bubble for large $\tilde{\alpha}$, in view of (A.8).

Any residual velocity of the liquid captured under the bubble will be small, as the liquid in the boundary layer is decelerated by the adverse pressure gradient outside the bubble and stopped entirely by the friction forces once under the bubble where no pressure force acts on the liquid. Effects of a residual velocity are automatically taken into account, if the displacement thickness of the boundary layer, by definition the hypothetical thickness of the layer at standstill in a further undisturbed flow field, is used to calculate the volume of liquid captured under the bubble. If the liquid in the microlayer is assumed to be at standstill the displacement thickness of the boundary layer must be equal to the microlayer thickness, which is given by

$$\frac{h_0(r_b)}{(4\nu_l t)} = \frac{Z_b}{\sqrt{2}}, \quad (A.35)$$

when (11) is rewritten with the help of (8) and (9). Comparing (A.35) and (A.34) at $\tilde{\alpha} = 1$ we find that Z_b will be of the order of magnitude

$$Z_b \simeq 0{\cdot}9. \quad (A.36)$$

Following this approach consistently, we consider in the analysis the liquid in the microlayer to be at rest. Changes in the original thickness of the microlayer, given by (11), will then occur through evaporation only.

Without evaporation, the thickness at each point would be given by (11) when r_b is replaced by $\tilde{r}$. We did not solve the problem of residual flow, but it is easy to see that it will cause a slight change in the radial distribution of the liquid volume under the bubble. Towards the outer edge the microlayer thickness will be larger than that given by (11), towards the centre of the bubble it will be slightly smaller. Neglect of the residual flow thus involves the neglect of a decrease in thickness additional to the decrease by evaporation.

CROISSANCE RAPIDE D'UNE BULLE DE VAPEUR A L'INTERFACE LIQUIDE–SOLIDE

Résumé—La croissance rapide des bulles de vapeur à l'interface liquide–solide comme dans les liquides bouillants est décrite par une solution d'affinité. Une bulle croît comme une hémisphère, le carré du rayon augmentant proportionnellement au temps, tandis qu'une fine couche de liquide quitte le solide sous la bulle. L'évaporation de cette couche contribue à la croissance et créé une région séche en son centre. La théorie est illustrée par quelques résultats expérimentaux. En appendice on présente une analyse de la couche limite sur la surface solide hors de la bulle. On montre que la séparation de cette couche limite ne peut se produire ce qui explique la présence d'une microcouche.

DAS SCHNELLE WACHSTUM EINER DAMPFBLASE AN EINER FLÜSSIG-FESTEN GRENZFLÄCHE

Zusammenfassung—Das schnelle Wachstum von Dampfblasen an einer flüssig-festen Grenzfläche, wie beim Sieden von Flüssigkeiten, wird mit Hilfe einer Ähnlichkeitslösung beschrieben. Eine Blase wächst als Halbkugel, das Quadrat des Radius wächst dabei proportional mit der Zeit, während gleichzeitig eine dünne Flüssigkeitsschicht auf der festen Oberfläche unter der Blase bestehen bleibt. Die Verdampfung von dieser Schicht trägt zur Wachstumsrate bei und erzeugt eine trockene Fläche in ihrem Zentrum. Die Theorie ist mit einigen experimentellen Ergebnissen veranschaulicht worden. Im Anhang wird eine Analyse über die Grenzschicht an der festen Oberfläche ausserhalb der Blase durchgeführt. Es wird gezeigt, dass eine Ablösung dieser Grenzschicht nicht auftritt, was die Anwesenheit der Mikroschicht erklärt.

ЬЫСТРЫЙ РОСТ ПАРОВОГО ПУЗЫРЬКА НА ПОВЕРХНОСТИ РАЗДЕЛА ЖИДКОСТЬ — ТВЁРДОЕ ТЕЛО

Аннотация—Быстрый рост пузырьков пара на поверхности раздела жидкость — твёрдое тело, как, например, в кипящих жидкостях, описывается уравнением автомодельности.

Пузырёк растёт как полусфера, квадрат радиуса которой увеличивается пропорционально времени, тогда как тонкий слой жидкости остаётся на твёрдой поверхности под пузырьком. Испарение из этого слоя создаёт сухую область в его центре и влияет на скорость роста пузырька. Теория иллюстрируется некоторыми экспериментальными данными. В приложении аналцтически рассмотрен пограничный слой на твёрдой поверхности за пределами пузырька. Показано, что отрыв этого пограничного слоя не происходит.